

# Home Detection Technique for Na<sup>+</sup> and K<sup>+</sup> in Urine Using a Self-Calibrated all-Solid-State Ion-Selective Electrode Array Based on Polystyrene–Au Ion-Sensing Nanocomposites

Fan Wang, Yujing Liu, Mengdi Zhang, Fan Zhang,\* and Pingang He

Cite This: *Anal. Chem.* 2021, 93, 8318–8325

Read Online

ACCESS |



Metrics &amp; More

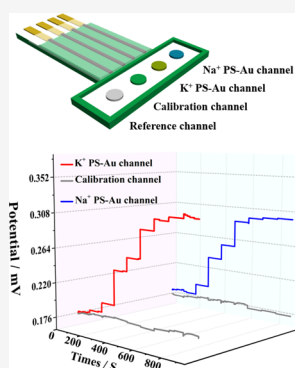


Article Recommendations



Supporting Information

**ABSTRACT:** An all-solid-state ion-selective electrode (ASS-ISE) array that is portable and easily miniaturized can meet the needs of home sensing devices for long-term health monitoring. However, their stability and accuracy are affected by the multistep modification required for ASS-ISE manufacturing and the complex background signal of real samples. In this study, a four-channel ISE array with the integration of a calibration channel has been developed based on polystyrene–Au (PS–Au) ion-sensing nanocomposites (PS–Au ISE array) for the home detection of Na<sup>+</sup> and K<sup>+</sup>. The nanocomposites combine target recognition function and ion-electron transduction function and could be modified on the channel surface by direct drop-casting, thus simplifying the preparation process and then improving the stability. Meanwhile, the integrated calibration channel could automatically deduct complex background signals in real sample analysis and thus improve the accuracy. As a result, the proposed self-calibrated PS–Au ISE array showed a near Nernstian behavior for Na<sup>+</sup> and K<sup>+</sup> in the range of  $1 \times 10^{-2} \text{ M} - 1 \times 10^{-4} \text{ M}$ , and the detection limits were  $6.8 \times 10^{-5} \text{ M}$  and  $5.5 \times 10^{-5} \text{ M}$  in artificial urine. The linear equations can be obtained according to the slopes and intercepts of Na<sup>+</sup> and K<sup>+</sup>, and thus, the concentration of the target ions can be directly read out by combining this PS–Au ISE array with the smart electronic device. Furthermore, the detection results of Na<sup>+</sup> and K<sup>+</sup> in human urine agreed well with those obtained by ICP–AES, suggesting that this proposed self-calibrated PS–Au ISE array is very suitable for home smart sensing devices, facilitating the health monitoring.



## INTRODUCTION

Sensors, one of the core technologies in artificial intelligence, are a front-end perception tool. Smart sensing devices that can measure multitargets have been used in environmental detection,<sup>1,2</sup> military engineering,<sup>3</sup> food management,<sup>4</sup> and personalized medicine and home diagnosis.<sup>5–7</sup> A variety of noninvasive devices such as band-aids,<sup>8</sup> contact lenses,<sup>9</sup> smart toilets,<sup>10</sup> and oral cavity patches<sup>11</sup> have been exploited in home diagnosis to monitor wound healing, eye health, urine composition, respiratory status, oral health, diet management, etc. Smart sensing devices, which are simple to operate and can realize real-time monitoring, have shown an irreplaceable position in home diagnosis. Among body fluids, urine is the most suitable detection object because it is easier to collect than sweat, more stable than saliva, and more noninvasive than blood. Therefore, home urinalysis can bring great convenience to persons who need long-term health monitoring.

All-solid-state ion-selective electrodes (ASS-ISEs) that are portable, low-cost, disposable, easily miniaturized, and flexibly designed can meet the needs of smart sensing devices.<sup>12,13</sup> As the first generation of ASS-ISEs, coated-wire electrodes were invented in the 1970s by Cattrall et al., to replace the conventional ion-selective electrodes.<sup>14</sup> However, they exhibit large signal drifts, due to the absence of ion-to-electron transducers and the formation of water layers. To improve the

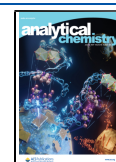
stability, various hydrophobic materials as the transition layer modified between the conductive substrate and ion-selective membrane have been proposed, such as conducting polymers, carbon materials, molecular redox couples, conductive metal–organic frameworks, and micro/nanonoble metal materials.<sup>15–18</sup> Meanwhile, paper-based screen-printing technology<sup>19,20</sup> and inkjet-printing technology<sup>21,22</sup> have been used to fabricate ASS-ISE arrays, which are highly demanded in smart sensing.

Nevertheless, ASS-ISEs still face a series of challenges in their application in smart sensing. It is known that the detected signal should be automatically converted into the content of target in the smart sensing device. Thus, it requires the high reproducibility of the signal, which is attributed to the excellent stability of the sensor. However, the commonly used ASS-ISEs are prepared by layers of assembly, and the complicated steps increase the differences between batches of electrodes.<sup>23,24</sup> Meanwhile, high accuracy with no interference from the

Received: March 19, 2021

Accepted: May 31, 2021

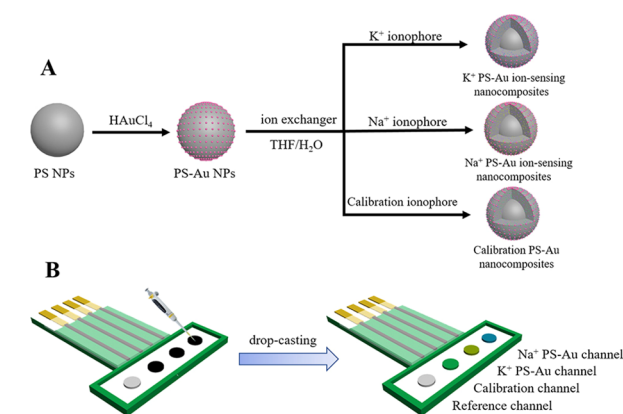
Published: June 7, 2021



background matrix of detected real samples is required. Usually, the background response was calibrated by the preprocessing method or standard solution method.<sup>25–27</sup> However, neither method is suitable for smart sensing. Therefore, it is highly urgent to improve the stability of ASS-ISEs and realize self-calibration of the background signal for their application in smart sensing devices.

To solve these problems, a four-channel ISE array, consisting of the Na<sup>+</sup> channel, K<sup>+</sup> channel, calibration channel, and reference channel, has been developed with self-calibration based on polystyrene–Au (PS–Au) ion-sensing nanocomposites (PS–Au ISE array) for the detection of Na<sup>+</sup> and K<sup>+</sup> in urine (Scheme 1). The synthesized nanocomposites integrate

**Scheme 1. Schematic Illustration of (A) Preparation of Functional PS–Au Ion-Sensing Nanocomposites and (B) Fabrication of the PS–Au ISE Array**



Au nanoparticles with ion–electron transduction function and the ionophore with recognition function and can be modified on the channel surface by direct drop-casting, thus simplifying electrode preparation steps and improving the stability of ISEs. Meanwhile, a calibration channel has been integrated in the four-channel ISE array fabricated on paper-based screen-printed carbon electrodes (SPCEs) to automatically deduct complex background signals in real sample analysis and thus improve the accuracy. The basic material of calibration nanocomposites is the same as that of Na<sup>+</sup>/K<sup>+</sup> ion-sensing nanocomposites. Therefore, the nonspecific response of the calibration channel to the background matrix of urine is considered to be consistent with that of sensing channels, presenting the same basic potential signals. Thus, the potentiometric response of sensing channels to the target ions can be self-calibrated by the calibration channel. This proposed PS–Au ISE array can directly detect Na<sup>+</sup> and K<sup>+</sup> in human urine samples without centrifugation or filtration pretreatment, so it is very suitable for home smart sensing devices, facilitating the health monitoring.

## EXPERIMENTAL SECTION

**Preparation of Amino-Functionalized Polystyrene Nanoparticles (PS–NH<sub>2</sub> NPs).** PS NPs were prepared using an emulsifier-free polymerization method reported before.<sup>28</sup> In a typical synthesis, 90 mL of deionized (DI) water, 10 g of styrene, and 0.1 g of acrylic acid monomer were added to a round-bottom flask equipped with a reflux condenser and a Teflon-coated mechanical stirring bar. The reaction mixture was stirred at room temperature for 1 h under a nitrogen

atmosphere prior to styrene polymerization. After the reaction mixture was heated to 75 °C, 5 mL of 20 mg/mL potassium persulfate solution was added followed by stirring for another 20 h under a nitrogen atmosphere at 75 °C. The obtained PS NPs were washed with DI water by centrifugation to remove the residual reactants. Then, 1 mL of 100 mg/mL PS NPs was added into 20 mL of a mixture of HNO<sub>3</sub>/H<sub>2</sub>SO<sub>4</sub> with a volume ratio of 3:2 and stirred at 40 °C for 3 h to obtain PS–NO<sub>2</sub> NPs. The product was washed with DI water until neutral. Next, PS–NH<sub>2</sub> NPs were obtained by adding the above PS–NO<sub>2</sub> NPs into a round-bottom flask containing a mixture of 1 g of Na<sub>2</sub>S<sub>2</sub>O<sub>4</sub> and 15 mL of 0.2 M NaOH and then stirring at 80 °C for 3 h. The final product was washed with DI water several times.

**Synthesis of Polystyrene–Au Nanoparticles (PS–Au NPs).** To prepare PS–Au NPs, 1 mL of 100 mg/mL PS–NH<sub>2</sub> NPs and 2 mL of 1% HAuCl<sub>4</sub> were first dispersed in 50 mL of DI water followed by heating to boiling with stirring. Then, 0.5 mL of 0.189 M trisodium citrate was rapidly added to the boiling solution, and the reaction was continued for another 2 h.

**Preparation of the Ion-Sensing Nanocomposites.** To prepare Na<sup>+</sup> ion-sensing nanocomposites, K<sup>+</sup> ion-sensing nanocomposites, and calibration nanocomposites,<sup>29</sup> 2.4 mg of sodium tetrakis[3,5-bis(trifluoromethyl)phenyl]borate (NaTFPB) dissolved in 0.1 mL of tetrahydrofuran (THF) solution containing 4 mg of 4-tert-Butylcalix[4]arenetetraacetic acid tetraethyl ester or valinomycin or *O*-xylylenebis(*N,N*-diisobutyldithiocarbamate) was pipetted and injected into 0.4 mL of 0.5 mg/mL PS–Au NPs. Then, the mixture was shaken for 2 h in a water-bath oscillator under 200 rpm at 25 °C followed by drying in a vacuum at 25 °C to volatilize THF. Afterward, these PS–Au ion-sensing nanocomposites were washed by centrifugation to remove the residual reactants and stored at 4 °C.

**Fabrication of the PS–Au ISE Array.** The PS–Au ISE array consists of a Na<sup>+</sup> PS–Au channel, a K<sup>+</sup> PS–Au channel, a calibration channel, and a reference channel, which was fabricated on the SPCEs. PP synthetic paper (0.5 mm in thickness) was used as the substrate of SPCEs. The silver ink as the conductive layer was printed on the sensing channels and connection ports followed by the printing of carbon layers on all electrode area (3 mm in diameter) and connection ports. The Ag/AgCl ink was printed on the reference channel. Finally, the insulating paste was printed. Curing at 100 °C for 20 min was needed after each printing. The SPCEs were then washed twice with ethanol and DI water.

The Na<sup>+</sup> PS–Au channel and K<sup>+</sup> PS–Au channel were prepared by casting 20 μL of Na<sup>+</sup> and K<sup>+</sup> PS–Au ion-sensing nanocomposites on the sensing electrode area, respectively. The calibration channel and reference channel were fabricated by dropping 20 μL of calibration PS–Au nanocomposites on the calibration electrode area and 25 μL of polyvinyl butyral resin (PVB) reference membrane cocktail (100 mg of NaCl, 250 mg of PVB, and 0.2 mg of multiwall carbon nanotubes in 2 mL of methanol)<sup>8</sup> on the Ag/AgCl reference electrode area, respectively. The Na<sup>+</sup> PVC selective membrane cocktail was prepared by dissolving 2 mg of Na ionophore, 1.2 mg of NaTFPB, 32.8 mg of PVC, and 65.6 mg of *O*-NPOE in 1 mL of THF, and the Na<sup>+</sup> PVC channel was obtained by drop-casting 25 μL of Na<sup>+</sup> PVC selective membrane cocktail on the sensing electrode area of SPCEs. The PS–Au ISE array was stored at 4 °C after vacuum drying at 25 °C for 5 h.

**Simultaneous Potentiometric Detection of Na<sup>+</sup> and K<sup>+</sup>.** Before the detections, the PS-Au ISE array was conditioned in 10<sup>-3</sup> M Na<sup>+</sup>/K<sup>+</sup> solution for 12 h. Then, open circuit potential measurements were carried out at 25 °C, and the content of Na<sup>+</sup> and K<sup>+</sup> was calculated using  $\Delta E$  values ( $\Delta E = E_{SC} - E_{CC}$ , where  $E_{SC}$  and  $E_{CC}$  represent the potential of the sensing channel and calibration channel, respectively). The response slope and intercept of the PS-Au ISE array for Na<sup>+</sup> and K<sup>+</sup> were first obtained in artificial urine, containing 1 mM uric acid, 5 mM creatinine, 160 mM urea, 1 mM calcium, 17.2 mM ammonium, 10 mM phosphate ions, and adjustable potassium and sodium concentration.<sup>30,31</sup> Then, the analysis of morning urine was performed directly without centrifugation or filtration pretreatment followed by reading out the concentration of Na<sup>+</sup> and K<sup>+</sup>. All data were repeated more than three times.

## RESULTS AND DISCUSSION

**Characterizations of the Ion-Sensing Nanocomposites.** The morphology of the prepared PS NPs and PS-Au NPs was observed by TEM. As shown in Figure 1A, PS NPs

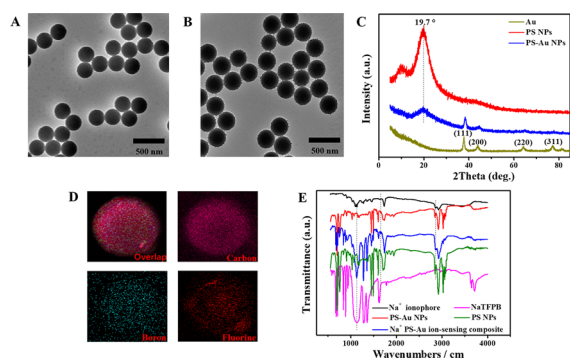


**Figure 1.** TEM images of (A) PS NPs and (B) PS-Au NPs; (C) XRD patterns of Au, PS NPs, and PS-Au NPs; (D) elemental mapping (overlap, carbon, boron, and fluorine) images of Na<sup>+</sup> PS-Au ion-sensing nanocomposites; (E) FT-IR spectra of the Na<sup>+</sup> ionophore, PS NPs, PS-Au NPs, NaTFPB, and Na<sup>+</sup> PS-Au ion-sensing nanocomposites.

presented a spherical shape with an average diameter of ~280 nm. After in-situ reduction of HAuCl<sub>4</sub> on the surface of PS NPs, the average diameter has no obvious change, but the surface became rough, and it can be seen that Au nanoparticles (~12 nm) were generated on the surface of PS (Figure 1B).

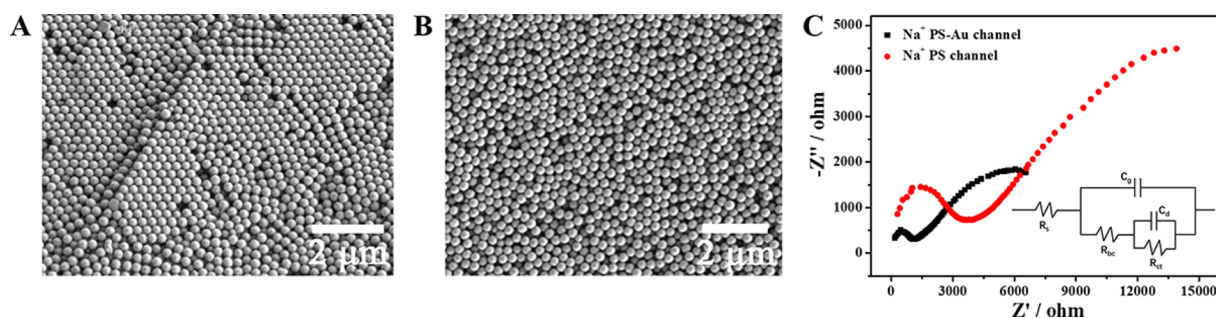


**Figure 2.** SEM images of (A) Na<sup>+</sup> PS ion-sensing nanocomposite-modified Na<sup>+</sup> channel, (B) Na<sup>+</sup> PS-Au ion-sensing nanocomposite-modified Na<sup>+</sup> channel, and (C) their corresponding impedance spectra in 0.1 M NaNO<sub>3</sub> solution with a 0.1 Hz–100 kHz frequency range and 10 mV excitation amplitude.

Figure 1C shows the X-ray diffraction (XRD) patterns of Au NPs, PS NPs, and PS-Au NPs. The four characteristic peaks at 37.8, 43.9, 64.2, and 77.2° are assigned to the (111), (200), (220), and (311) planes of Au nanoparticles (JCPDS No. 04-0784), respectively. In the diffraction patterns of PS-Au NPs, the peaks of Au NPs (37.8°) and PS NPs (19.7°) are observable, indicating the successful preparation of the nanoparticles.<sup>32</sup>

Figure 1D shows the elemental mapping (overlap, carbon, boron, and fluorine) images of Na<sup>+</sup> PS-Au ion-sensing nanocomposites. It could be observed that Na<sup>+</sup> PS-Au ion-sensing nanocomposites contain boron and fluorine elements, indicating that NaTFPB dissolved in PS-Au nanocomposites successfully. The same characterization results were also presented for K<sup>+</sup> PS-Au ion-sensing nanocomposites and calibration nanocomposites (data not shown).

PS NPs, PS-Au NPs, the Na<sup>+</sup> ionophore, NaTFPB, and Na<sup>+</sup> PS-Au ion-sensing nanocomposites were further characterized by FT-IR spectroscopy (Figure 1E). In the spectrum of PS NPs, the absorption peaks at 1601, 1492, and 1451 cm<sup>-1</sup> were attributed to C=C stretching vibration of the benzene skeleton, and the adsorption peaks at 3060, 3024, 754, and 698 cm<sup>-1</sup> correspond to C-H stretching vibration and C-H out-plane bending vibration of benzene, which are all characteristic absorption of PS.<sup>28</sup> The FT-IR spectrum of PS-Au NPs was basically unchanged compared with that of PS NPs because the Au nanoparticles have no FT-IR absorption. In the spectrum of Na<sup>+</sup> PS-Au ion-sensing nanocomposites, not only the characteristic adsorption peaks of PS-Au could be observed but also those of the Na<sup>+</sup> ionophore and NaTFPB, which indicated that the Na<sup>+</sup> ionophore and NaTFPB were successfully dissolved in PS-Au ion-sensing nanocomposites. Meanwhile, the FT-IR spectra of K<sup>+</sup> PS-Au ion-sensing nanocomposites in comparison with the K<sup>+</sup> ionophore, NaTFPB, PS NPs, and PS-Au NPs and calibration nanocomposites in comparison with *O*-xylylenebis(*N,N*-diisobutyl-dithiocarbamate) (calibration ionophore), NaTFPB, PS NPs, and PS-Au NPs are exhibited in Figure S1, indicating the successful preparation of K<sup>+</sup> PS-Au ion-sensing nanocomposites and calibration nanocomposites.

**Characterizations of the PS-Au ISE Array.** The morphology of the Na<sup>+</sup> PS ion-sensing nanocomposite-modified Na<sup>+</sup> channel (Na<sup>+</sup> PS channel) and the Na<sup>+</sup> PS-Au ion-sensing nanocomposite-modified Na<sup>+</sup> channel (Na<sup>+</sup> PS-Au channel) was observed by SEM. As shown in Figure 2A,B, Na<sup>+</sup> PS ion-sensing nanocomposites and Na<sup>+</sup> PS-Au ion-sensing

nanocomposites were evenly and tightly arranged on the surface of the channel, forming a film of nanoparticles.

The electrochemical impedance spectra of the Na<sup>+</sup> PS-Au channel and Na<sup>+</sup> PS channel were recorded in 0.1 M NaNO<sub>3</sub>, and an equivalent circuit was further established (Figure 2C). It can be seen that there are five parameters in this equivalent circuit, including the solution resistance ( $R_s$ ), the bulk membrane resistance, and contact resistance between the ion-sensing nanocomposites and the underlying carbon layer of SPCEs ( $R_{bc}$ ), geometric capacitance ( $C_g$ ), charge-transfer resistance ( $R_{ct}$ ), and double-layer capacitance ( $C_d$ ).<sup>18,33</sup>  $R_{bc}$  could represent the diameter of the semicircle in the high-frequency region of the Nyquist plots. Fitting the impedance spectra to the equivalent circuit by ZsimpWin software affords the values of these parameters (Table S1). Clearly, the Na<sup>+</sup> PS-Au channel features a smaller  $R_{bc}$  and  $R_{ct}$  and a larger  $C_d$ , which indicates that it is more suitable for fabricating ISE arrays.

To investigate the applicability of synthesized ion-sensing nanocomposites as the recognition element and ion-to-electron transducer, the potentiometric responses of the Na<sup>+</sup> PS-Au channel were measured in 0.1–1 × 10<sup>-6</sup> M NaNO<sub>3</sub> solutions (Figure 3A). It can be seen that the potential values increase

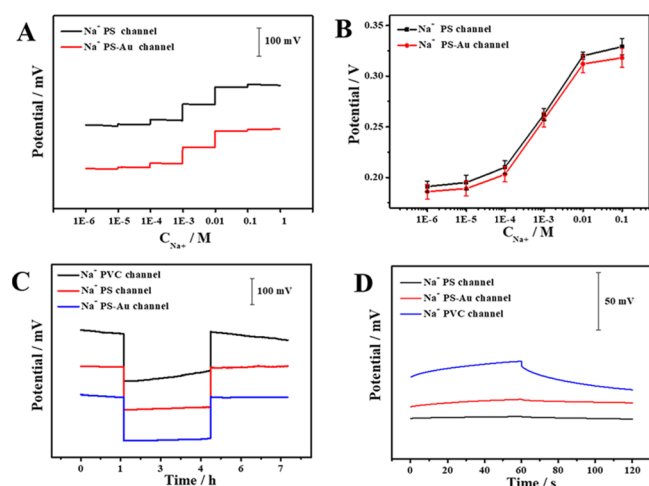


**Figure 3.** (A) Time-dependent potentiometric response of the Na<sup>+</sup> PS-Au channel and Na<sup>+</sup> PS channel; (B) relationships between the logarithmic concentrations of Na<sup>+</sup> and potential values; (C) water layer tests and (D) chronopotentiograms of the Na<sup>+</sup> PS-Au channel, Na<sup>+</sup> PS channel, and Na<sup>+</sup> PVC channel.

with the increased concentration of Na<sup>+</sup>. A linear response can be obtained in a range of 0.1–10 mM with ~20 s of stationary time (Figure 3B). The Na<sup>+</sup> PS channel almost presents the same potentiometric response characteristics.

Although Au NPs could improve the potentiometric performance of PS ion-sensing nanocomposites little, they contribute significantly to the stability of the PS-Au channel, which was evaluated by the water layer test and chronopotentiometry. The formation of the water layer in the ASS-ISEs is one of the main factors causing potential signal drift because the ionic composition of the water layer would be changed by the transmembrane ion fluxes. The water layer test was performed by recording the potentiometric response of the electrode in main ion solution, interfering ion solution, and main ion solution, successively. If there is a water layer, the potential signal drift could be observed during the solution replacement.<sup>33</sup> Herein, the water layer test of the Na<sup>+</sup> PS-Au

channel was carried out using 1 × 10<sup>-2</sup> M NaNO<sub>3</sub> and 0.1 M KNO<sub>3</sub> as the main ion solution and interfering ion solution with the test results of the Na<sup>+</sup> PS channel and Na<sup>+</sup> PVC channel for comparison. As shown in Figure 3C, the Na<sup>+</sup> PVC channel presents 42 mV of positive potential drift in 3.5 h of 0.1 M KNO<sub>3</sub> replacement. However, the values obtained for the Na<sup>+</sup> PS channel and Na<sup>+</sup> PS-Au channel were only 18 and 9 mV, respectively. It has been reported that a higher plasticizer content in the PVC membrane could facilitate the uptake of water.<sup>34</sup> Therefore, the observed potential drift could be attributed to the formation of a water layer and the absence of an ion-to-electron transducer. However, uniform PS-based nanocomposites do not contain plasticizers, greatly decreasing the formation rate of the water layer. Furthermore, since Na<sup>+</sup> PS-Au ion-sensing nanocomposites with high double-layer capacitance can accelerate ion-electron conduction and prevent charge blocking, the potential signal of the Na<sup>+</sup> PS-Au channel is almost constant during the replacement of 0.1 M KNO<sub>3</sub>, indicating that the water layer could be largely reduced.

Figure 3D exhibits the chronopotentiograms of the Na<sup>+</sup> PS-Au channel, Na<sup>+</sup> PS channel, and Na<sup>+</sup> PVC channel in 1 × 10<sup>-3</sup> M NaNO<sub>3</sub> with the application of +1 nA for 60 s and -1 nA for another 60 s.<sup>35</sup> The obtained corresponding potential drift at 60 s is 1.5, 6.6, and 14 mV. Clearly, PS-based channels are more stable than the PVC channel and the Na<sup>+</sup> PS-Au channel shows the best potential stability,<sup>36</sup> which are consistent with the water layer test results.

The sensitivity of the PVB reference channel to chloride ions was checked by testing potentiometric responses of the PVB reference channel with Ag/AgCl/KCl(3 M) as a reference in KCl and NaCl solution at different concentrations. As shown in Figure S2, the potential change could be negligible in a range of 1.0 × 10<sup>-4</sup> M – 1.0 M for both NaCl and KCl, indicating that the PVB reference channel has low potential sensitivity to chloride ions and ionic strength, and could provide the constant potential.

**Self-Calibration.** The difference in the background matrix of a real sample may cause large errors in potentiometric determination, thus decreasing the accuracy. In general, this error could be calibrated by the preprocessing sample method or standard solution method. However, these calibration methods are not suitable for home detection. Therefore, a calibration channel was designed in this PS-Au ISE array to deduct the influence of the background matrix on potential signal in home detection. To fabricate the calibration channel, calibration PS-Au nanocomposites were coated on the channel surface by drop-casting. Like K<sup>+</sup>/Na<sup>+</sup> PS-Au ion-sensing nanocomposites, they contain PS-Au NPs, ion-exchangers, and ionophores, but the type of ionophore is different. In detail, PS-Au NPs were chosen as the base material, and Ag<sup>+</sup> ionophores ((*O*-xylylenebis(*N,N*-diisobutyldithiocarbamate)) that did not respond to the target ion were selected as the calibration ionophore to prepare calibration PS-Au nanocomposites. An ionophore is necessary for the nanocomposites because lipophile ions in the sample would cause interference. As the calibration ionophore, it should not respond to target ions and the content of the main ions recognized by the calibration ionophore in urine must be much lower than the detection limit of the calibration channel in the PS-Au ISE array. Thus, its potential change is just caused by the background matrix in the urine sample through nonspecific adsorption. The content of Ag<sup>+</sup> in urine is extremely low, so the Ag<sup>+</sup> ionophore was selected as the calibration ionophore in

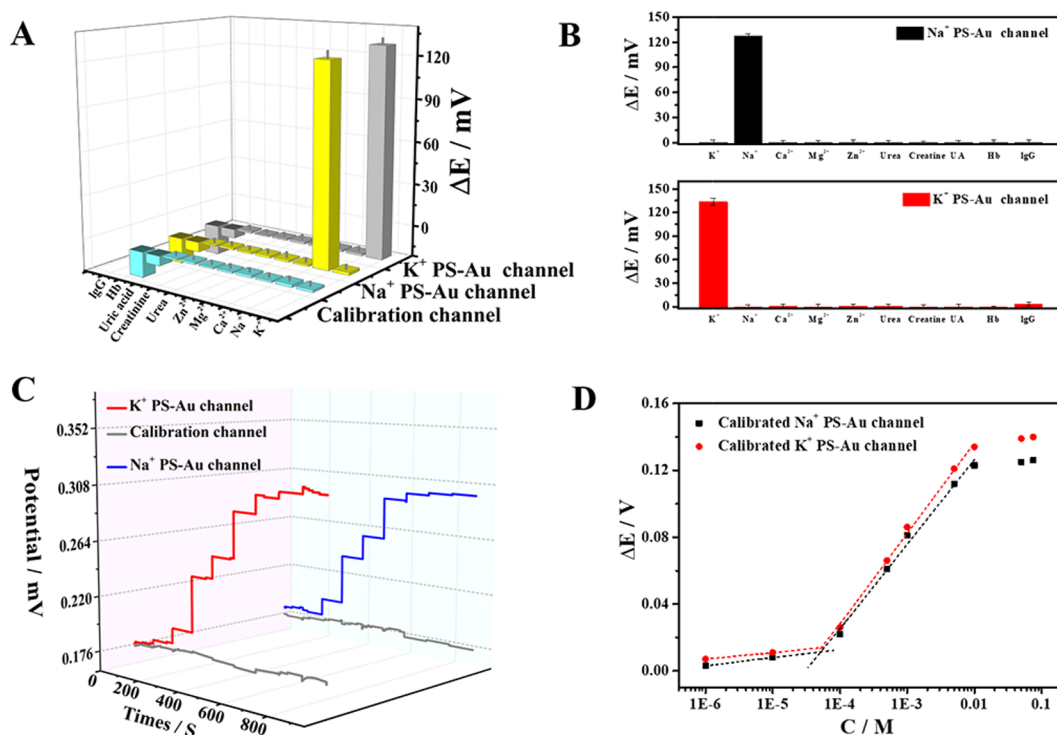


**Figure 4.** (A) Potentiometric responses of the Na<sup>+</sup> PS-Au channel, K<sup>+</sup> PS-Au channels, and calibration channels to 10 mM PBS (pH = 6) containing 10 mM Na<sup>+</sup>, 10 mM K<sup>+</sup>, 10 mM Ca<sup>2+</sup>, 10 mM Mg<sup>2+</sup>, 10 mM Zn<sup>2+</sup>, 1 mM uric acid, 5 mM creatinine, 160 mM urea, 1 mg/mL Hb, and 1 mg/mL IgG, respectively; (B) potential difference between the Na<sup>+</sup>/K<sup>+</sup> PS-Au channel and calibration channel; (C) potentiometric response curves of the Na<sup>+</sup> PS-Au channel, K<sup>+</sup> PS-Au channel, and calibration channel in artificial urine containing 0.075–1 × 10<sup>-6</sup> M Na<sup>+</sup> or K<sup>+</sup>; (D) relationships between the calibrated potentiometric responses of the Na<sup>+</sup> PS-Au channel and K<sup>+</sup> PS-Au channel and the concentrations of Na<sup>+</sup>/K<sup>+</sup>.

this work. To prove further the calibration function of calibration PS-Au nanocomposites, their zeta potential was detected and compared with that of K<sup>+</sup>/Na<sup>+</sup> PS-Au ion-sensing nanocomposites. As shown in Figure S3, these three kinds of nanocomposites present almost the same zeta potentials, revealing that the difference in ionophore types does not affect their surface charged property. Therefore, the changes in the basic potential of the sensing channel and calibration channel caused by the nonspecific adsorption of macromolecules such as proteins in the background matrix of urine can be consistent. That is the reason why the potentiometric response of sensing channels to the target ions can be self-calibrated by the calibration channel.

To investigate the self-calibration performance of the fabricated PS-Au ISE array, the potentiometric responses of the Na<sup>+</sup> PS-Au channel, K<sup>+</sup> PS-Au channel, and calibration channel were recorded in 10 mM PBS containing K<sup>+</sup>, Na<sup>+</sup>, Mg<sup>2+</sup>, Zn<sup>2+</sup>, Ca<sup>2+</sup>, urea, uric acid, creatinine, hemoglobin porcine (Hb), and human immunoglobulin G (IgG), respectively (Figure 4A). Obviously, the Na<sup>+</sup> PS-Au channel and K<sup>+</sup> PS-Au channel show specific potentiometric response to Na<sup>+</sup> and K<sup>+</sup>, respectively, while the calibration channel does not respond to Na<sup>+</sup> or K<sup>+</sup>. On the other hand, the addition of nontarget ions, creatinine, uric acid, and urea almost does not change the potential of K<sup>+</sup> or Na<sup>+</sup> PS-Au channels. However, after adding 1 mg/mL Hb or IgG, the potential values of all three channels changed by almost the same amount, probably attributed to the adsorption of charged protein macromolecules on the channel surface. Moreover, due to the different isoelectric points of Hb (~7) and IgG (~8), the potential values show a decrease of ~7 and ~18 mV, respectively. This indicates that proteins with different

isoelectric points have different effects on the potentiometric response. Thus, the self-calibration is very necessary for ASS-ISEs in the detection of real samples.

The effect of protein on the response slope was also tested by measuring 0.1–1 × 10<sup>-6</sup> M Na<sup>+</sup> or K<sup>+</sup> containing different proteins, respectively. As shown in Table S2, the presence of protein in the test solution does not affect the response slopes. The possible reason is that the protein is uniformly distributed on the channel surface but does not block the entire electrode surface, so the transport of ions between the solution and PS-Au ISE array is not affected.<sup>25</sup>

Since the background matrix causes the same potential changes of the calibration channel and sensing channels and does not affect the response slope of sensing channels to the target ions, the potential signal of sensing channels can be self-calibrated by directly subtracting the calibration channel value without any additional procedures. As clearly shown in Figure 4B, the obtained calibrated signal  $\Delta E$  ( $\Delta E = E_{SC} - E_{CC}$ , where  $E_{SC}$  and  $E_{CC}$  represent the potential of the sensing channel and calibration channel), is completely caused by the target ions, and the influence of the background matrix on the detection with the PS-Au ISE array is almost negligible. Consequently, the calibration channel can be used to eliminate the influence of the background matrix and calibrate the basic potential of sensing channels, realizing the more accurate detection of urine samples.

**Potentiometric Response Performance of the PS-Au ISE Array.** To obtain the best potentiometric response performance of the PS-Au ISE array, the amount of PS-Au ion-sensing nanocomposites was first optimized by chronopotentiometry. Using Zeta View, it could be known that 0.1 mg of Na<sup>+</sup> PS-Au ion-sensing nanocomposites contains 3.2 × 10<sup>10</sup>

nanoparticles. The SEM image in Figure 2B shows that the nanocomposites are dispersed on the channel surface in a densely packed manner, so by approximating PS-Au ion-sensing nanocomposites as equal diameter spheres and using the densest way that each sphere is tangent to six spheres, we found that it needs 4  $\mu\text{L}$  of 0.1 mg/mL  $\text{Na}^+$  PS-Au ion-sensing nanocomposites at least to lay a layer on the channel surface. Thus, the potential drift values of the  $\text{Na}^+$  PS-Au channel modified with 0.1 mg/mL nanocomposites in the volume range of 4–24  $\mu\text{L}$  were investigated. As shown in Figure S4, when the amount of  $\text{Na}^+$  PS-Au ion-sensing nanocomposites increases, the potential drift value decreases first and reaches a plateau at an amount of 20  $\mu\text{L}$ . That is to say, the  $\text{Na}^+$  PS-Au channel arranged with five layers of  $\text{Na}^+$  PS-Au ion-sensing nanocomposites exhibits the best performance. The same refers to the  $\text{K}^+$  PS-Au channel. Therefore, the PS-Au ISE array modified with 20  $\mu\text{L}$  of PS-Au ion-sensing nanocomposites for each channel was used for the potentiometric determination of artificial urine (Table S3).<sup>30,31</sup>

Figure 4C shows the potentiometric response of the PS-Au ISE array in artificial urine containing 0.075– $1 \times 10^{-6}$  M  $\text{Na}^+$  or  $\text{K}^+$ . It can be seen that the potential values of the  $\text{Na}^+$  PS-Au channel and  $\text{K}^+$  PS-Au channel increase with the concentration increase of  $\text{Na}^+$  and  $\text{K}^+$ , respectively, while the calibration channel does not respond to the target ions. The linear relationship between the logarithmic concentration of target ions and the calibrated potential value of the PS-Au sensing channel by the calibration channel can be further obtained in a range of  $1 \times 10^{-2}$  M –  $1 \times 10^{-4}$  M (Figure 4D), and the potentiometric response parameters of  $\text{Na}^+$  and  $\text{K}^+$  are presented in Table 1. The linear equation can be obtained

**Table 1. Potentiometric Response Parameters of  $\text{Na}^+$  and  $\text{K}^+$  by the Self-Calibrated PS-Au ISE Array**

| target ion    | slope (mV/decade) | intercept (mV)  | detection limit (M)  | $R^2$ |
|---------------|-------------------|-----------------|----------------------|-------|
| $\text{Na}^+$ | $50.3 \pm 1.3$    | $221.5 \pm 5.6$ | $6.8 \times 10^{-5}$ | 99.5  |
| $\text{K}^+$  | $53.5 \pm 1.2$    | $235.3 \pm 6.0$ | $5.5 \times 10^{-5}$ | 99.2  |

according to the slope and intercept, and thus, the concentration of the targets can be directly read out by combining with the smart electronic device. The performances of the PS-Au ISE array were further compared with other reported ISEs for the detection of  $\text{Na}^+$  and  $\text{K}^+$ . As shown in Tables S4 and S5, the response slope of this PS-Au ISE array is comparable with that of other reported ISEs, and the PS-Au ISE array demonstrates a relatively wider response range. More importantly, this ISE array improves the stability and accuracy of home sensing by using multifunctional PS-Au nanocomposites, which can be modified on the channel surface by one drop-casting, and designing a calibration channel to automatically deduct background signals caused by the nonspecific adsorption.

**Selectivity.** The selectivity of the PS-Au ISE array was investigated by the separate solution method in  $1 \times 10^{-3}$  M target ions and interfering ions. The logarithmic selectivity coefficients were calculated using the Nicolskii–Eisenman equation:  $\log_{I,J}^{\text{pot}} = \frac{(E_J - E_I)Z_I F}{2.303RT} + \log \frac{a_I}{a_J^{Z_I/Z_J}}$  ( $E_I$  and  $E_J$  represent the potential value of target ions and interfering ions, respectively;  $a_I$  and  $a_J$  represent the activity of target ions and interfering ions, respectively;  $Z_I$  and  $Z_J$  represent the

charge number of target ions and interfering ions, respectively).<sup>37</sup> Table 2 shows  $\log_{\text{Na},J}^{\text{pot}}$  and  $\log_{\text{K},J}^{\text{pot}}$  tested by the PS-Au

**Table 2. Logarithmic Selectivity Coefficients of Sensing Channels in the PS-Au ISE Array with and without Self-Calibration**

| interfering ions | $\log_{\text{Na},J}^{\text{pot}}$ |                     | $\log_{\text{K},J}^{\text{pot}}$ |                     |
|------------------|-----------------------------------|---------------------|----------------------------------|---------------------|
|                  | with calibration                  | without calibration | with calibration                 | without calibration |
| $\text{Na}^+$    |                                   |                     | $-3.9 \pm 0.6$                   | $-3.8 \pm 0.4$      |
| $\text{K}^+$     | $-3.2 \pm 0.4$                    | $-3.1 \pm 0.5$      |                                  |                     |
| $\text{Ca}^{2+}$ | $-5.3 \pm 0.7$                    | $-5.7 \pm 0.7$      | $-4.6 \pm 0.8$                   | $-5.1 \pm 0.6$      |
| $\text{Mg}^{2+}$ | $-5.5 \pm 0.8$                    | $-5.2 \pm 0.5$      | $-4.9 \pm 1.1$                   | $-5.3 \pm 0.4$      |
| $\text{Zn}^{2+}$ | $-4.9 \pm 1.0$                    | $-4.7 \pm 0.8$      | $-4.3 \pm 0.7$                   | $-4.6 \pm 0.4$      |
| $\text{Cu}^{2+}$ | $-5.3 \pm 0.6$                    | $-4.8 \pm 0.6$      | $-5.1 \pm 0.5$                   | $-4.7 \pm 0.4$      |

ISE array with and without self-calibration. Clearly, the PS-Au ISE array shows the satisfactory selectivity to the tested interfering ions even without calibration. Moreover, there is barely a change in the selectivity coefficients when the potential of the sensing channel was calibrated, which benefits from the fact that the calibration channel does not respond to the target ions. Therefore, this PS-Au ISE arrays can achieve highly selective determination of  $\text{Na}^+$  and  $\text{K}^+$ .

**Reproducibility and Stability.** The reproducibility was evaluated by testing the slopes and intercepts of 10 PS-Au ISE arrays. As indicated in Figure 5A, the average slope and intercept of the  $\text{Na}^+$  PS-Au channel are 50.7 mV/decade and 221.6 mV with relative standard deviations (RSDs) of 2.3 and 2.4%, respectively. Values of 53.6 mV/decade with an RSD of 2.5% and 236.8 mV with an RSD of 2.2% are determined for the  $\text{K}^+$  PS-Au channel, revealing the satisfactory reproducibility of the PS-Au ISE array between batches.

The stability of the PS-Au ISE array was investigated by detecting the slope and intercept variations within 60 days. From Figure 5B, it could be observed that the slope and intercept do not change significantly, and the RSDs were less than 2.6%, indicating no detachment of nanocomposites, probably because the average size of the nanocomposites is about 280 nm, and such a small sized particle could present good fastness on the channel surface. Therefore, the prepared PS-Au ISE array has a high stability and could meet the requirement of home smart sensing.

**Detection of  $\text{Na}^+$  and  $\text{K}^+$  in Human Urine.** The physiological ranges of  $\text{Na}^+$  and  $\text{K}^+$  in human urine are 130–260 mM and 25–125 mM, respectively. They could be detected using the self-calibrated PS-Au ISE array without centrifugation or filtration in advance. In detail, 2 mL of fresh morning urine was first diluted 30 times with DI water, and then, the open circuit potential was performed with an 8-channel electrochemical workstation with the activated PS-Au ISE array. The concentrations of target ions were calculated relying on the linear correlation between the logarithmic concentration of target ions and the calibrated potential value. Table S6 shows the potential values of  $\text{Na}^+$  and  $\text{K}^+$  in urine of a healthy individual over a week. The corresponding concentrations of  $\text{Na}^+$  and  $\text{K}^+$  are calculated and exhibited in Table 3, showing that the results tested by the proposed PS-Au ISE array agree well with the measurements by ICP-AES.

Although the linear range in this work does not cover the concentration levels of  $\text{Na}^+$  and  $\text{K}^+$  in the actual samples, they

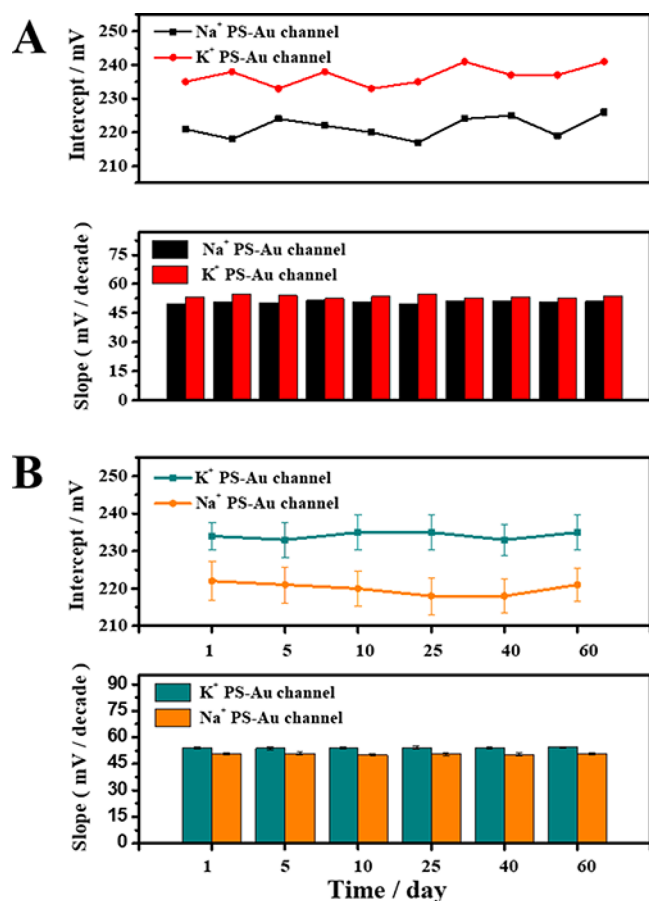


**Figure 5.** (A) Reproducibility of 10 self-calibrated PS-Au ISE arrays; (B) stability of the self-calibrated PS-Au ISE array within 60 days.

**Table 3. Detection of Na<sup>+</sup> and K<sup>+</sup> in Human Urine Samples with the Self-Calibrated PS-Au ISE Array and ICP-AES**

| time  | urine Na <sup>+</sup> |              | urine K <sup>+</sup> |              |
|-------|-----------------------|--------------|----------------------|--------------|
|       | present method (mM)   | ICP-AES (mM) | present method (mM)  | ICP-AES (mM) |
| Day 1 | 195 ± 9               | 183          | 69 ± 6               | 78           |
| Day 2 | 189 ± 6               | 195          | 45 ± 12              | 51           |
| Day 3 | 168 ± 12              | 162          | 69 ± 6               | 60           |
| Day 4 | 209 ± 6               | 228          | 81 ± 15              | 87           |
| Day 5 | 165 ± 12              | 162          | 78 ± 12              | 87           |
| Day 6 | 198 ± 15              | 207          | 69 ± 9               | 63           |
| Day 7 | 165 ± 12              | 177          | 78 ± 12              | 66           |

just need dilution before the detection with the PS-Au ISE array. More importantly, the PS-Au ISE array has achieved excellent stability and accuracy, which are urgent problems to be solved in home sensing. Consequently, it shows great potential for home sensing applications.

## CONCLUSIONS

In summary, a novel PS-Au ISE array based on PS-Au ion-sensing nanocomposites and SPCEs with a calibration channel has been proposed for home detection of Na<sup>+</sup> and K<sup>+</sup>. The PS-Au ion-sensing nanocomposites give this array the advantages of easy preparation, good conductivity, high stability, and excellent potentiometric response performance. Meanwhile, the introduction of the calibration channel has been proved to deduct background signals automatically, improving the

accuracy. In addition, the calibrated potential signals performed by the PS-Au ISE array presented a near Nernstian behavior of Na<sup>+</sup> and K<sup>+</sup> in the range of  $1 \times 10^{-2} \text{ M} - 1 \times 10^{-4} \text{ M}$ , with a slope of  $50.3 \pm 1.3 \text{ mV/decade}$  and intercept of  $221.5 \pm 5.6 \text{ mV}$  for Na<sup>+</sup> and  $53.5 \pm 1.2 \text{ mV/decade}$  and  $235.3 \pm 6.0 \text{ mV}$  for K<sup>+</sup>. Finally, this PS-Au ISE array was further applied to detect Na<sup>+</sup> and K<sup>+</sup> in human urine samples, and the results were validated by ICP-AES. The satisfactory reproducibility and accuracy indicate that this PS-Au ISE array can be applied to long-term monitoring of human urine samples, showing high potential in developing home smart sensing devices.

## ASSOCIATED CONTENT

### Supporting Information

The Supporting Information is available free of charge at <https://pubs.acs.org/doi/10.1021/acs.analchem.1c01203>.

Reagents and instruments; FT-IR spectra of K<sup>+</sup>/calibration PS-Au ion-sensing nanocomposites; fitted EIS parameters of the Na<sup>+</sup> PS-Au channel and Na<sup>+</sup> PS channel; characterizations of the PVB reference channel; zeta potentials of Na<sup>+</sup>/K<sup>+</sup>/calibration PS-Au nanocomposites; response slopes of the Na<sup>+</sup>/K<sup>+</sup> PS-Au channel in Na<sup>+</sup> or K<sup>+</sup> solution containing different proteins; optimization of the dosage of PS-Au ion-sensing nanocomposites; composition of artificial urine; performance comparison between the PS-Au ISE array and other reported ISEs; potential responses of Na<sup>+</sup> and K<sup>+</sup> by the PS-Au ISE array (PDF)

## AUTHOR INFORMATION

### Corresponding Author

Fan Zhang – School of Chemistry and Molecular Engineering, East China Normal University, Shanghai 200241, P.R. China; [orcid.org/0000-0003-4229-3916](https://orcid.org/0000-0003-4229-3916); Phone: +86-21-54340049; Email: [fzhang@chem.ecnu.edu.cn](mailto:fzhang@chem.ecnu.edu.cn)

### Authors

Fan Wang – School of Chemistry and Molecular Engineering, East China Normal University, Shanghai 200241, P.R. China

Yujing Liu – School of Chemistry and Molecular Engineering, East China Normal University, Shanghai 200241, P.R. China

Mengdi Zhang – School of Chemistry and Molecular Engineering, East China Normal University, Shanghai 200241, P.R. China

Pingang He – School of Chemistry and Molecular Engineering, East China Normal University, Shanghai 200241, P.R. China

Complete contact information is available at:

<https://pubs.acs.org/10.1021/acs.analchem.1c01203>

### Notes

The authors declare no competing financial interest.

## ACKNOWLEDGMENTS

This work was financially supported by the National Natural Science Foundation of China (Grant No. 22074042).

## ■ REFERENCES

- (1) Yu, H. A.; Lee, J.; Lewis, S. W.; Silvester, D. S. *Anal. Chem.* **2017**, *89*, 4729–4736.
- (2) Yuan, D.; Anthis, A. H. C.; Afshar, M. G.; Pankratova, N.; Cuartero, M.; Crespo, G. A.; Bakker, E. *Anal. Chem.* **2015**, *87*, 8640–8645.
- (3) Lim, H. B.; Ma, D.; Wang, B.; Kalbarczyk, Z.; Iyer, R. K.; Watkin, K. L. *Int. Conf. Body Sens. Netw.* **2010**, 246–249.
- (4) Yu, J.; Tang, W.; Wang, F.; Zhang, F.; Wang, Q.; He, P. *Sens. Actuator B: Chem.* **2020**, *311*, 127857.
- (5) Anastasova, S.; Crewther, B. T.; Bembnowicz, P.; Curto, V. F.; Ip, H. M.; Rosa, B. M. G.; Yang, G. Z. *Biosens. Bioelectron.* **2017**, *93*, 139–145.
- (6) Sun, A. C.; Yao, C.; Venkatesh, A. G.; Hall, D. A. *Sens. Actuator B: Chem.* **2016**, *235*, 126–135.
- (7) Zhang, D.; Lu, Y.; Zhang, Q.; Liu, L.; Li, S.; Yao, Y.; Jiang, J.; Liu, G. L.; Liu, Q. *Sens. Actuator B: Chem.* **2016**, *222*, 994–1002.
- (8) Gao, W.; Emaminejad, S.; Nyein, H. Y. Y.; Challa, S.; Chen, K.; Peck, A.; Fahad, H. M.; Ota, H.; Shiraki, H.; Kiriya, D.; Lien, D. H.; Brooks, G. A.; Davis, R. W.; Javey, A. *Nature* **2016**, *529*, 509–514.
- (9) Kim, J.; Kim, M.; Lee, M. S.; Kim, K.; Ji, S.; Kim, Y. T.; Park, J.; Na, K.; Bae, K. H.; Kyun Kim, H.; Bien, F.; Young Lee, C.; Park, J. U. *Nat. Commun.* **2017**, *8*, 14997.
- (10) Park, S. M.; Won, D. D.; Lee, B. J.; Escobedo, D.; Esteva, A.; Aalipour, A.; Ge, T. J.; Kim, J. H.; Suh, S.; Choi, E. H.; Lozano, A. X.; Yao, C.; Bodapati, S.; Achterberg, F. B.; Kim, J.; Park, H.; Choi, Y.; Kim, W. J.; Yu, J. H.; Bhatt, A. M.; Lee, J. K.; Spittler, R.; Wang, S. X.; Gambhir, S. S. *Nat. Biomed. Eng.* **2020**, *4*, 624–635.
- (11) Lee, Y.; Howe, C.; Mishra, S.; Lee, D. S.; Mahmood, M.; Piper, M.; Kim, Y.; Tieu, K.; Byun, H. S.; Coffey, J. P.; Shayan, M.; Chun, Y.; Costanzo, R. M.; Yeo. *Proc. Natl. Acad. Sci. U. S. A.* **2018**, *115*, 5377–5382.
- (12) Hu, J.; Stein, A.; Bühlmann, P. *Angew. Chem., Int. Ed.* **2016**, *55*, 7544–7547.
- (13) Parrilla, M.; Cuartero, M.; Crespo, G. A. *TrAC Trends Anal. Chem.* **2019**, *110*, 303–320.
- (14) James, H. J.; Carmack, G.; Freiser, H. *Anal. Chem.* **1971**, *43*, 856–1906.
- (15) El-Rahman, M. K. A.; Rezk, M. R.; Mahmoud, A. M.; Elghobashy, M. R. *Sens. Actuator B: Chem.* **2015**, *208*, 14–21.
- (16) Jansod, S.; Wang, L.; Cuartero, M.; Bakker, E. *Chem. Commun.* **2017**, *53*, 10757–10760.
- (17) Liu, C.; Jiang, X.; Zhao, Y.; Jiang, W.; Zhang, Z.; Yu, L. *Electrochim. Acta* **2017**, *231*, 53–60.
- (18) Mendecki, L.; Mirica, K. A. *ACS Appl. Mater. Interfaces* **2018**, *10*, 19248–19257.
- (19) Roy, S.; Davidpur, M.; Hanein, Y. *ACS Appl. Mater. Interfaces* **2017**, *9*, 35169–35177.
- (20) Lan, W. J.; Zou, X. U.; Hamed, M.; Hu, J.; Parolo, C.; Maxwell, E. J.; Bühlmann, P.; Whitesides, G. M. *Anal. Chem.* **2014**, *86*, 9548–9553.
- (21) Li, L.; Pan, L.; Ma, Z.; Yan, K.; Cheng, W.; Shi, Y.; Yu, G. *Nano Lett.* **2018**, *18*, 3322–3327.
- (22) Ruecha, N.; Chailapakul, O.; Suzuki, K.; Citterio, D. *Anal. Chem.* **2017**, *89*, 10608–10616.
- (23) Zeng, X.; Qin, W. *Anal. Chim. Acta* **2017**, *982*, 72–77.
- (24) Guzinski, M.; Jarvis, J. M.; Pendley, B. D.; Lindner, E. *Anal. Chem.* **2015**, *87*, 6654–6659.
- (25) Joon, N. K.; He, N.; Wagner, M.; Cárdenas, M.; Bobacka, J.; Lisak, G. *Electrochim. Acta* **2017**, *252*, 490–497.
- (26) Joon, N. K.; He, N.; Ruzgas, T.; Bobacka, J.; Lisak, G. *Anal. Chem.* **2019**, *91*, 10524–10531.
- (27) Lisak, G.; Arnebrant, T.; Lewenstam, A.; Bobacka, J.; Ruzgas, T. *Anal. Chem.* **2016**, *88*, 3009–3014.
- (28) Xiao, C.; Liu, X.; Mao, S.; Zhang, L.; Lu. *J. Appl. Surf. Sci.* **2017**, *394*, 378–385.
- (29) Xie, X.; Zhai, J.; Bakker, E. *J. Am. Chem. Soc.* **2014**, *136*, 16465–16468.
- (30) Parra, K. N.; Gul, S.; Aquino, J. M.; Miwa, D. W.; Motheo, A. J. *Solid State Electrochem.* **2015**, *20*, 1001–1009.
- (31) Sarigul, N.; Korkmaz, F.; Kurultak, I. *Sci. Rep.* **2019**, *9*, 20159.
- (32) Wang, Y.; Liu, X.; Deng, G.; Wang, Q.; Zhang, L.; Wang, Q.; Lu, J. *J. Mater. Chem. B* **2017**, *5*, 4221–4232.
- (33) Li, J.; Yin, T.; Qin, W. *Anal. Chim. Acta* **2015**, *876*, 49–54.
- (34) Lindfors, T.; Sundfors, F.; Höfler, L.; Gyurcsányi, R. E. *Electroanalysis* **2009**, *21*, 1914–1922.
- (35) Hu, J.; Zou, X. U.; Stein, A.; Bühlmann, P. *Anal. Chem.* **2014**, *86*, 7111–7118.
- (36) Paczosabator, B.; Cabaj, L.; Piech, R.; Skupien, K. *Anal. Chem.* **2013**, *85*, 10255–10261.
- (37) Wang, Z.; Tang, W.; Yu, J.; Zhang, F.; He, P. *J. Electroanal. Chem.* **2019**, *835*, 137–142.